Corrosion Science 167 (2020): 108528

DOI: https://doi.org/10.1016/j.corsci.2020.108528

Engineering nanostructured cell micropatterns on Ti6Al4V by selective ion-beam inhibition of pitting

R. López[1,2], M.D. Ynsa [1,3], P.J. de Pablo[2], F. Lim[4], M. Manso Silván[1 *]

1 Departamento de Física Aplicada and Instituto de Ciencia de Materiales Nicolás Cabrera, Universidad Autónoma de Madrid, 28049 Madrid, Spain.

2 Departamento de Física de la Material Condensada and Instituto de Ciencia de Materiales Nicolás Cabrera, Universidad Autónoma de Madrid, 28049 Madrid, Spain.

3 Centro de Microanálisis de Materiales, Universidad Autónoma de Madrid, 28049 Madrid, Spain.

4. Departamento de Biología Molecular, Universidad Autónoma de Madrid, 28049 Madrid, Spain.

*corresponding author: miguel.manso@uam.es, tel: +34 914974918

Abstract:

We have modified Ti6Al4V at the micro and nanoscale by using ion beam irradiation with 5 MeV Si^+ ions through 1D micromasks. The passivation layer on irradiated areas inhibits hydrofluoric acid induced etching, leading to pitting contrasts. Surface microscopies and spectroscopies reveal that the nanotopographic modification correlates with a preferential titanium etching, and lead to dual surface free energy properties. The patterns are able to induce guidance of olfactory ensheathing glia cells, mainly through inhibition of adhesion on nanostructured areas, and could be attractive substrates for the induction of stimuli to neural cells under non voltaic polarization.

Keywords: high energy ion beam implantation, pitting, Ti6Al4V, cell guidance, olfactory ensheathing glia cells.

1 Introduction

Titanium alloys are present nowadays in many advanced mechanical applications, such as in the fuselage of aircrafts, sports tools and in endo-prostheses, to cite a few examples [1]. Ti has two allotropic configurations: α, with hexagonal close-packed crystal structure; and β, with body-centered cubic structure. By adding aluminium and vanadium as main α and β stabilizers, respectively, alpha-beta alloys can be stabilized at room temperature. Ti6Al4V (90 Ti, 6 Al, 4 V wt.%) is the most common α+β titanium alloy, which exhibits high strength while maintaining high temperature processability (especially welcome when biomedical applications are in focus) [2]. In the field of regenerative medicine, the performance of titanium endoprostheses is sustained (besides the mechanical properties of the alloys) by their high biocompatibility, which derives from the presence of a protective oxide layer with slow pitting kinetics in physiological conditions [3].

The topography of titanium plays a relevant role in the cyto and histocompatibility of the alloy, which has justified an engineering of the surfaces from the nano to the micometer scale [4]. The topography affects directly and indirectly the surface free energy; by inducing capillary effects and by modifying the surface chemistry via the deployment of a thicker oxide layer [5]. These overall changes in surface free energy are sensed by different cells and tissues and determine the bioadhesive or non-fouling response of the alloy; while macrotopographies induce enhanced biointegration [6], the presence of highly hydrophilic titania nanoconstructs induces cell-repellent behaviour [7, 8].

In spite of the protecting effect of the oxide, since the expected lifetime of implants often exceeds 10 years, the Ti alloy suffers a progressive corrosion. This slow process can be prevented by different chemical and physical corrosion prevention processes [9],

which lead most often to the formation of an additional passivation layer. Among the chemical methods, electrochemically designed interfaces [10], sol-gel ceramic [11] and bioceramic [12] coatings and biopolymer-metal nanocomposite layers [13], have been used to reinforce passivation. From the side of the physical techniques, laser annealing [14], ultrasonic hardening [15], electron beam melting [16], magnetron sputtering nitruration [17], and ion implantation in the KeV [18] and MeV [19, 20] ion energy range have been proposed for the same purpose.

Interestingly, periodic micro and nanotopographies have become a relevant instrument to carry out fundamental and applied studies related to cell adhesion control [21, 22]. From the exploration of basic metabolic changes in guided/polarized cells leading to enhanced biocompatibility [23], applications of micro/nano-patterned titanium based materials evolve to the production of anisotropic tissues [24]. It has also been shown that micropatterning is an outstanding intermediate step to produce un-cracked anticorrosive bioceramic films on metallic devices [25]. In this direction, surface micro/nanotexturing of Ti surfaces has been induced by laser processes [26]. In the current work, we propose that a sequential process of selective high energy ion bombardment and HF induced etching, can be used to create alternative nanotopographic micropatterns on Ti6Al4V alloys. We propose that by such micropatterning one can not only improve the integration response and assimilation of an implant, but also propose new devices, such as cell guides for neuronal interconnections [27].

In this sense, we studied in this work an immortalized line of glial cells derived from human olfactory bulb (TS14 Olfactory Ensheathing Cells, OECs) [28]. We previously characterized this cell line and confirmed that they maintain the neuro-regenerative and axonal growth promoting properties of primary OECs. These cells have been demonstrated to promote functional and structural recovery when transplanted into

the injured spinal cord [29]), with indications of similar potential in clinical studies. Indeed, in a limited number of patients with spinal cord injuries there were promising indications of the potential of OEC transplants to restore some voluntary motor activity [30]. These results set the interest for a deeper study of the interaction of OECs with structural implantable biomaterials such as Ti6Al4V alloys.

2 Experimental

2.1 Ti6Al4V micropatterning.

The fabrication of nanotopographic micropatterns on Ti6Al4V was performed after independent optimization of the high energy ion implantation and pitting processes following the fabrication scheme of Figure 1, which led to their final use as cell guiding supports. Squared pieces of Ti6Al4V (1x1 cm^2) were cut and polished with ascendant grades of silicon carbide sandpaper (P2000) and final smoothing with a velvet cloth until a specular polishing was obtained. The Ti6Al4V surfaces were finally washed in trichloroethylene, acetone and ethanol (EtOH) in subsequent ultrasound baths of 20 min at 40°C.

The Ti6Al4V substrates were irradiated in a tandetron accelerator with 5 MeV Si^+ ions at fluences of 1×10^{14}, 1×10^{15} or 5×10^{15} cm^{-2}. When irradiating with high energy ions, the loss of energy is generally dominated by the electronic braking power, caused by the interactions between the ion and the electrons of the material. These electronic processes lead to a soft and quasi-continuous loss of energy, leaving the direction of the projectile almost invariant during this first stage of implantation [31]. Selective irradiation was achieved by placing 1D copper TEM grids (30-50 μm wide stripes) on the Ti6Al4V surface. Etching was performed in hydrofluoric acid (HF 48% vol) diluted in absolute

EtOH (at 1:1, 1:2 or 1:4 volume ratios) for 5 s. The etching stopped upon immersion of the Ti6Al4V in absolute EtOH.

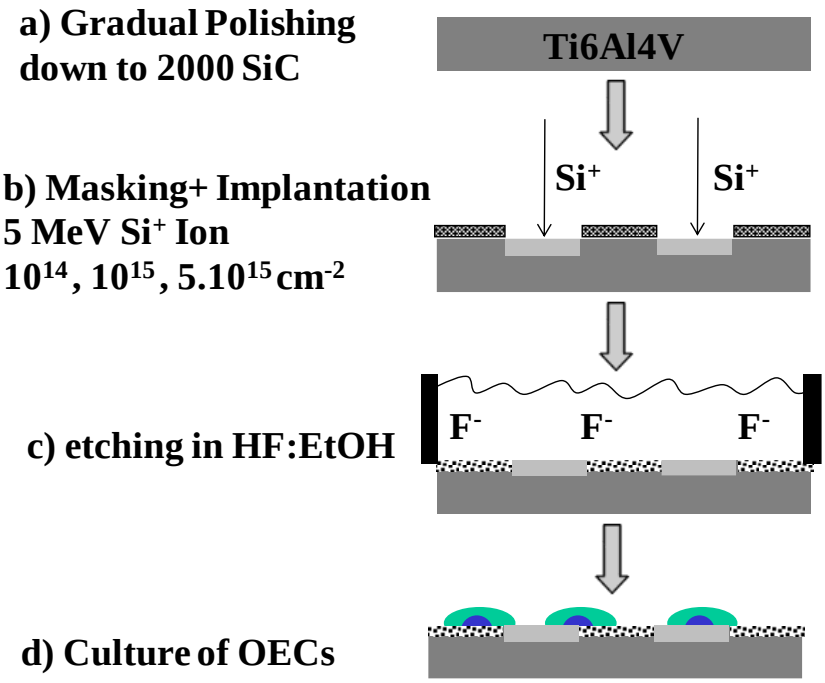

Figure 1. Fabrication scheme of the micropatterned Ti6Al4V alloys. From top to bottom: a) Surface polishing of Ti6Al4V, b) masked irradiation with 5^{+} MeV ions, c) etching in HF with controlled dilution in EtOH and time and d) application in cell culture. HF, hydrofluoric acid; EtOH, ethanol, OECs, olfactory ensheathing cells.

2.2 Characterization Techniques.

Ellipsometry was performed on polished and irradiated Ti6Al4V samples in a J.A. Woollam Co. VASE ellipsometer. Analyses were performed in the 200−1500 nm range at 70º incidence angle. The results were fitted to a simple TiO_2/Ti6Al4V model using experimental determinations of the optical functions for both materials and allowing a diffusing interface between both materials.

The morphology of the Ti6Al4V surface after ion implantation and etching was observed by field emission scanning electron microscopy (FE-SEM, Philips XL- 30FEG). X-ray photoelectron spectra (XPS) were obtained in a SPECS GmbH Spectrometer upon irradiation with monochromatic Al-Kα X-rays (hν=1486.6 eV) and photoelectron analysis in normal take-off angle (40 eV pass energy). The data were processed using CasaXPS v16R1 (Casa Software, UK) taking the C1s hydrocarbon component at 285.00 eV as binding energy (BE) reference and using Gaussian-Lorentzian function (G/L = 30) for core level envelopes. Atomic Force Microscopy (AFM) was carried out in a Dulcinea microscope from Nanotec Electronica, employing PPPNCH-20 cantilevers with L=125μm, W=30 μm and K∼24.8 N/m. A PDLFAST- 11 piezotube was used to acquire (in air and tapping mode) 5 μm^2 and 75 μm^2 images with 1024 points for each line. AFM images were acquired and analysed using WSxM [32].

Wetting was evaluated by sessile-drop Water Contact Angle (WCA) measurements performed in a KSV 100 system using droplet volumes of 3 μl. On the micropatterns, dew contrast images were obtained in a Zeiss optical microscope.

2.2 Olfactory ensheathing glial cells.

Olfactory ensheathing cells (OECs) used in this study were the immortalized cell line TS14 derived from olfactory bulb [28]. Stable transfectants of these cells expressing green fluorescent protein (GFP) from Aequorea victoria were used to allow monitoring of live cells on the opaque titanium substrates by fluorescence microscopy. OECs were grown in 10 cm dishes (total area of 56.7 cm^2), at 37 °C with 5% CO_2 to confluence, after which medium was removed and OECs were washed with phosphate buffered saline (PBS) and lifted from the dish with TrypLE enzyme (Thermofisher 12563029). Finally, cells were cultured on the Ti6Al4V samples in Dulbecco's Modified Eagle Medium

(DMEM) supplemented with 10% fetal calf serum (FCS) at 37 °C with 5% CO_2. Cells were incubated for 24 hours to allow adherence to the substrates, after which medium was removed and the cells were fixed for 15 minutes at 4°C with 4% paraformaldehyde. Nuclei were stained with 4′,6- diamidino-2-phenylindole (DAPI) diluted in PBS and applied for 10 minutes in the dark. For selected samples additional experiments were performed by staining the actin cytoskeleton with phalloidin-Alexa 647 (Thermofisher A22287) following the same procedure. Finally, substrates were washed three times with PBS and mounted with mowiol and glass coverslips. Fluorescence microscopy was performed using an Olympus IX-UCB inverted microscope equipped with a CCD camera.

2 Results

3.1 Irradiation and etching of Ti6Al4V.

The formation of Ti6Al4V micropatterns was initiated with the irradiation of the polished surfaces with 5 MeV Si^+ ions. To evaluate the effects of the irradiation process, a set of Ti6Al4V samples was irradiated homogeneously on the surface at different fluences of 10^{14}, 10^{15} and 5×10^{15} cm^{-2}. These surfaces were firstly characterized by ellipsometry as a sensitive optical technique for irradiation-induced damage. The results of the derived values of refractive index (n) and extinction coefficient (k) for the irradiations with different fluence are presented in Figure 2 (note curves are shifted to facilitate comparison). The experimental results are shown along a simulation for a simple model consisting of a TiO_2 surface layer of variable thickness on top of a Ti substrate, which are interfaced by a soft transition layer. The agreement between experimental and fitted curves is reasonable in the visible range, although deviations exist in the infrared range. It can be observed that the most remarkable difference between the samples is a deeper valley in the extinction function at circa 290 nm, in concomitance with an

increasing refractive index peak at circa 260 nm, for an increasing irradiation fluence. This observation can be interpreted in terms of the simulated data as an effect of an increasing thickness of the surface TiO_2 layer for increasing irradiation fluence. The data of thickness obtained for the different layers (transition and TiO_2) from the simulated curves is plotted in figure 2.b. The trend illustrates that there is an increasing thickness of oxidised material on the surface upon increasing irradiation and that irradiation at fluences of 5×10^{15} cm^{-2} enhances the rate of formation of the surface oxide layer. Overall, the total oxide surface layer increases from 2.5 nm for the non-irradiated sample to circa 9 nm for the one irradiated at 5×10^{15} cm^{-2}. The relevance of this effect on the micropatterning process was put in evidence by creating irradiation contrasts with areas exposed to the highest fluence and areas fully protected by a metallic mask from the irradiation.

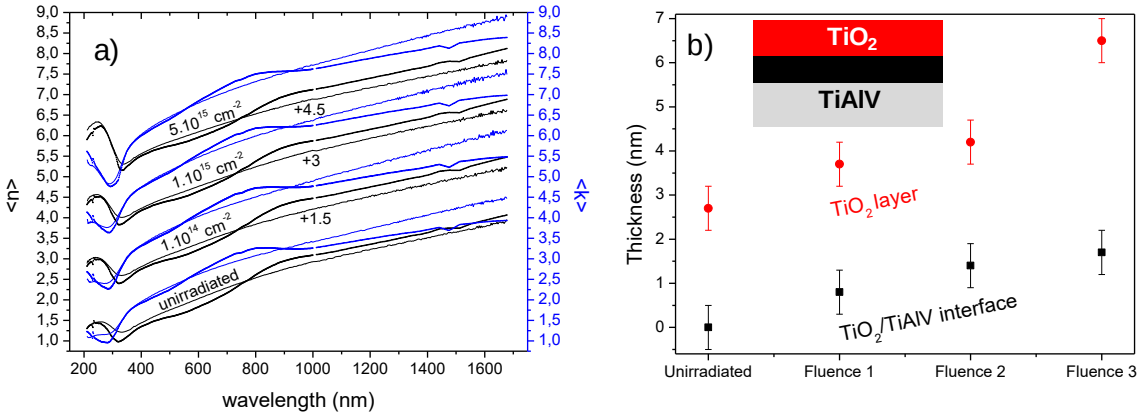

Figure 2. a) Values of *n* (left axis) and *k* (right axis) optical functions (note shift to facilitate comparison) of the Ti6Al4V substrate after implantation with 5 MeV Si^+ ions at fluences ranging from 0 to 5×10^{15} cm^{-2}. b) Plot of the thickness of the TiO_2 and interfacial oxide formed upon irradiation as obtained from the simulation of the spectra with the layer model illustrated in the inset.

The effect of the irradiation contrast on Ti6Al4V, prior to any etching, could be visualized by two wetting measurements. Firstly, the WCA of the two surfaces with highest irradiation contrast was measured. The WCA contrast between intensively irradiated areas and non-irradiated areas was circa 20º, the irradiated samples being more hydrophobic as illustrated in Figure 3.a. We next prepared surfaces with selective irradiation in micropatterned areas to see if the induced damage was enough to produce dew point contrasts at room temperature. Figure 3.b shows how, for an equivalent partial vapour pressure of water, the irradiated area of a micropatterned sample (right) resists dew, while non-irradiated (masked) areas are dew-covered, as a pristine polished Ti6Al4V substrate (left). This result suggested that the micropatterns induced by irradiation could lead to areas with different susceptibility to etching/pitting.

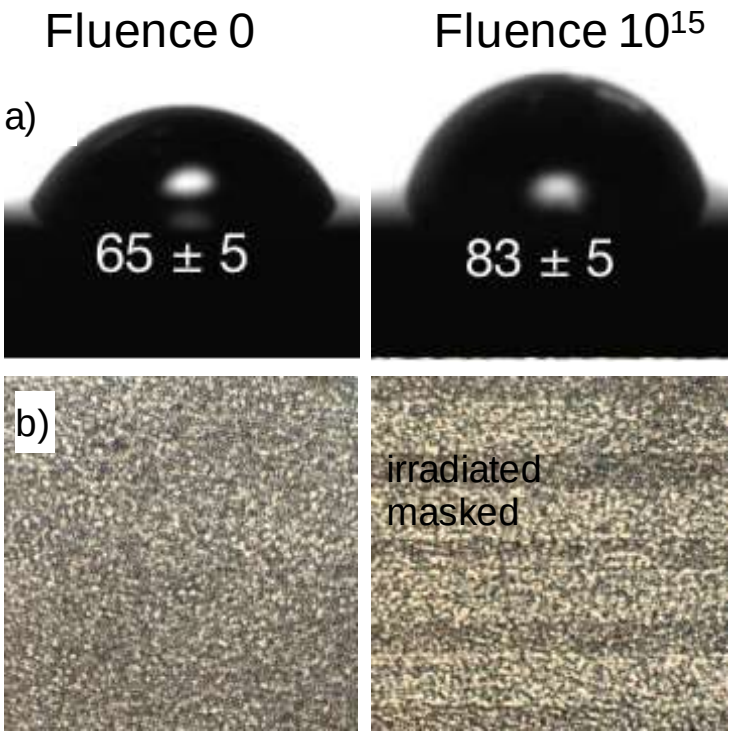

Figure 3. a) WCA of Ti6Al4V substrates before and after implantation with 5 MeV Si^+ at 10^{15} cm^{-2}. b) Dew test performed on as polished (left) and micropatterned Ti6Al4V (right) after irradiation with 5 MeV Si^+ at $10^{15}.cm^{-2}$.

Finally, prior to the formation of the nanotopographic micropatterns we studied the effects on wetting of different etching conditions for samples irradiated with 5 MeV Si^+ at 10^{15} cm^{-2}. The WCA evolution for 50 s was measured on irradiated surfaces after etching in solutions with HF:EtOH volume fractions of 1:1, 1:2 and 1:4 for 5 s. The results are plotted in figure 4, showing that the wetting trend is relatively similar for all samples. However, the most concentrated conditions were more respectful of the originally hydrophobic nature of the irradiated samples, while the more diluted samples led to a more hydrophilic behaviour. This is in agreement with previous studies in which, the high surface tension of the HF acidic solution is more determinant of the final surface properties of the etched surface than the concentration of the acid used to induce the etching [33].

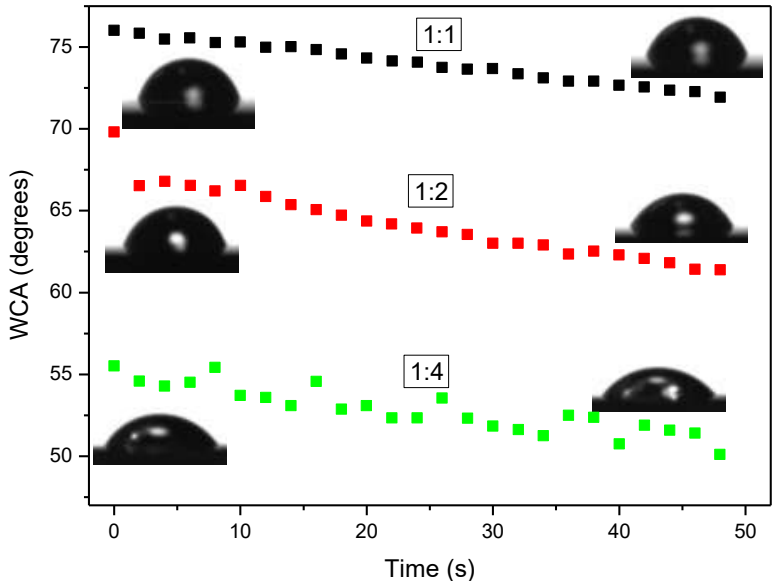

Figure 4. WCA measurements on the surfaces of Ti6Al4V alloys after irradiation with 5 MeV Si^+ ions at 10^{15} cm^{-2} and etching in HF:etanol solutions at volume rates of 1:1, 1:2 and 1:4 and exposure for 5 s.

To gain an insight into the changes in the chemical composition of the surface upon HF etching we performed an XPS study of two model surfaces, one as irradiated

and the other after irradiation and etching in a 1:2 HF:EtOH solution. The survey spectra were used to quantify the surface stoichiometry of the treated Ti6Al4V alloys, which contained O, an aliphatic C fingerprint, Ti, Al, V and F (this latter, only in the case of the etched sample). The most relevant aspect from the stoichiometric analysis is the increase of surface aluminium content from 4.1% to 5.1%. This rise was however much more remarkable when viewed in relative terms to the overall metallic elements. In fact, the Al/(Al+Ti+V) ratio increased from 0.29 to 0.40. The surface composition was also enriched in V, but in a less drastic way, with a transition of the V/(Al+Ti+V) ratio from 0.075 to 0.071 after the etching process. This indicates a slight preferential etching of V from Ti6Al4V during HF etching.

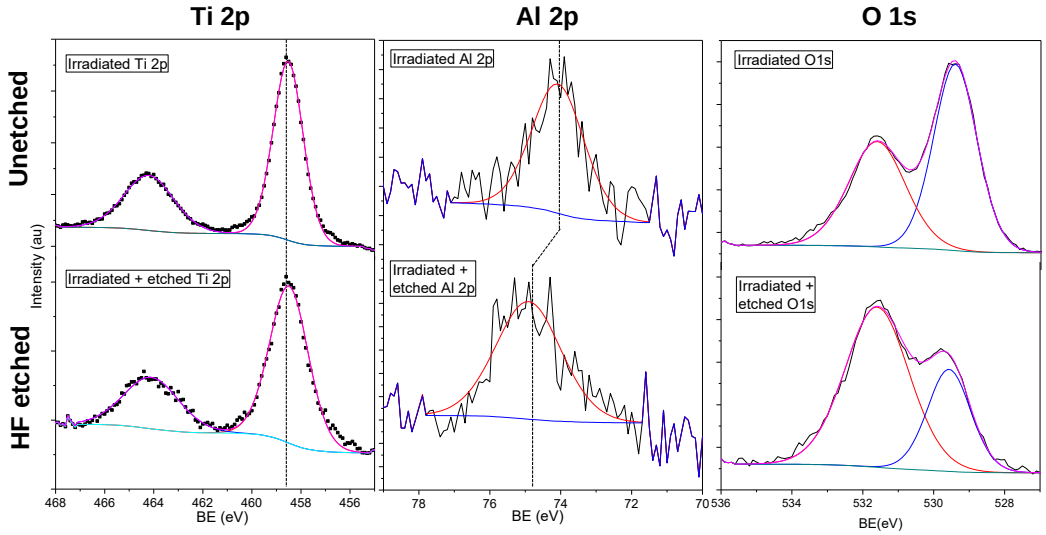

Figure 5 Ti2p, Al2p and O1s XPS core level spectra from the surfaces of Ti6Al4V irradiated with 5 MeV Si^{+} ions at 10^{15} cm^{-2} before (top) and after etching in HF:EtOH 1:2 solution (bottom).

From the point of view of the chemical state of the metallic elements, the most remarkable aspect concerns again the Al fraction of the alloy. Figure 5 shows the Ti 2p

and Al 2p core level spectra of the Ti6Al4V samples as irradiated and after irradiation and etching. The Ti 2p peaks show the well resolved spin orbit splitting with the characteristic profile of a TiO_2 phase. However, for the Al peaks that was not the case. The BE shift of the irradiated sample is in agreement with a partially oxidized Al (BE of 74.0 eV), which turns into a consolidated Al_2O_3 for the sample after wet-etching (BE of 74.7 eV). This observation can be related to the stoichiometric increase of surface Al, and points to its role as corrosion retardant by producing surface stable Al_2O_3 phases. In fact, the modification of the components of the O1s spectrum in figure 5 further support this idea. The high BE component at 531.6 eV (attributed to stable Al_2O_3 phases, and to F bonding) suffers after the etching treatment a relative increase with respect to the low BE component at 529.6 eV (attributed to carbonate and TiO_2). The surface segregation and enrichment of Al on Ti6Al4V and related alloys is a well-known issue on the surfaces of both annealed [34] and irradiated alloys [35]. Our study shows that the activation of the wet-etching further enriches the surface alumina content, in agreement with what observed during thermal annealing [36] and is justified by the higher reactivity of oxygen with Al than Ti. This higher reactivity has been previously evidenced layeredternary compounds (TiAlN) [37].

3.2 Micro-nano patterning of Ti6Al4V.

To evaluate the different effects of the consecutive irradiation and etching effects on a single surface, micropatterns were created by masking the Ti6Al4V surfaces with TEM grids during ion irradiation. The morphologic effects after the two step lithographic process were analysed using FE-SEM and AFM. Figure 6 shows the resulting surface structures observed for irradiation at 10^{15} cm^{-2} and subsequent HF etching in EtOH solutions with decreasing F^- ion concentration. Figure 6.a shows the effects with the most

concentrated HF solution, where microscale bodies resembling grain boundary structures emerge from a relatively flat surface. It is worth noting that this flat background surface presents a clear contrast between the irradiated and masked areas. The irradiated zone presents a second level of roughness, which appears as a flat area in the masked zone. By reducing the HF concentration to HF:EtOH 1:2 (Figure 6.b), the contrast between the two areas becomes more evident, with remaining flat domains on the irradiated areas that are fully etched out on the masked region. At the lowest HF concentration considered (Figure 6.c), the surface etching selectivity becomes drastic, with a clear pattern towards more intense and smaller pitting on the masked areas with respect to the irradiated ones. The low magnification image (figure 6.d) clearly illustrates the topographic effect on the two different areas.

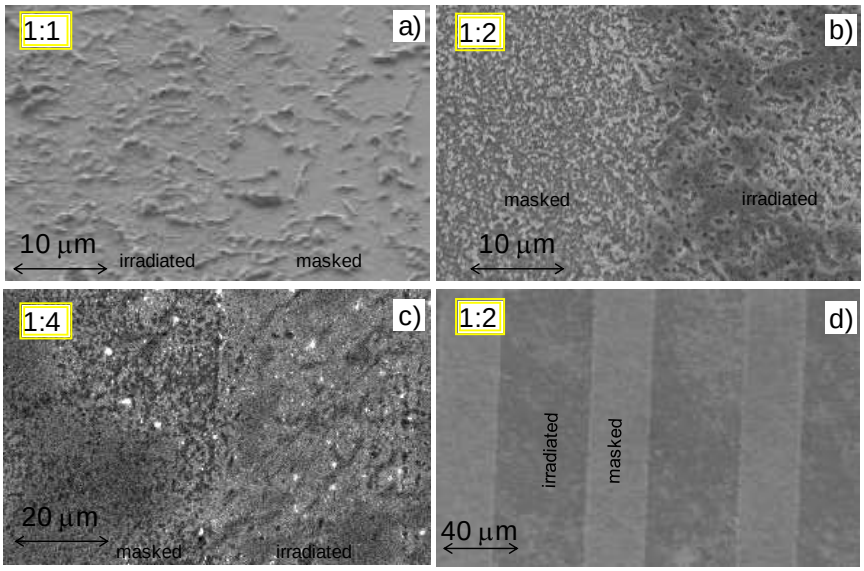

Figure 6. SEM images from the surface of Ti6Al4V after selective irradiation with 5 MeV Si^{+} ions at 1×10^{15} cm^{-2} and etching in 1:1 (a), 1:2 (b) and 1:4 (c) HF:EtOH. (d) Lower magnification image with general view of the secondary electron contrast induced by etching in 1:2 HF:EtOH.

The surface induced topographic effects were analysed with more detail using AFM (Figure 7). The 5x5 μm^2 images show that at the nm scale the longitudinal edge between irradiated and masked areas is not perfectly defined. The surfaces present globular features of different sizes (Figs. 7a-c), which are smaller on the irradiated areas, and even smaller if etched at the lowest HF concentration. However, all the surfaces show lateral steps in the form of different z-planes at the edge between masked and irradiated areas. Relevantly, the step height after fitting planes is also considerably smaller for the HF:EtOH 1: 4 sample (less than 20 nm height versus more than 50 nm for the other two etching conditions). This is illustrated by the green topography profile in figure 7.d, showing a RMS roughness in the irradiated areas which is comparable to the analysed in the original polished surface (5±1 nm). To further examine the contrasting nanotopography, a statistical analysis of the nanotopography of the different samples was performed.

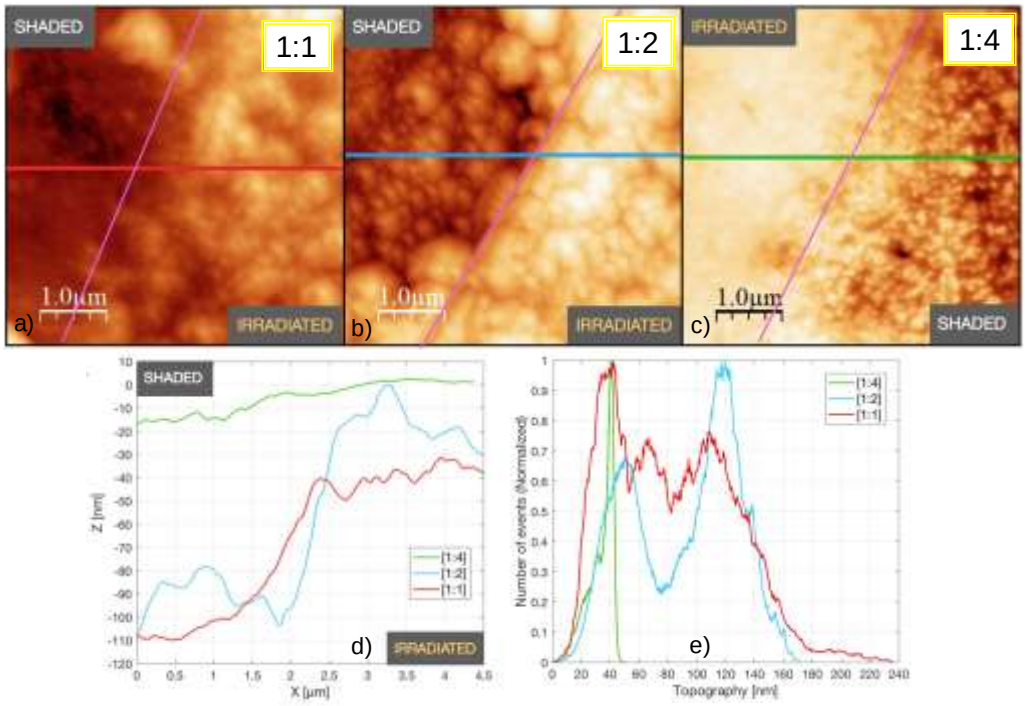

Fig 7: AFM images at the edge of unirradiated/irradiated (5 MeV Si^+ ions at 1×10^{15} cm^{-2}) Ti6Al4V areas after etching with different HF:EtOH solutions as labelled (a-c). Surface

profile across the edge of irradiation for Ti6Al4V surfaces obtained with different HF:EtOH solutions (the colours of the lines in the AFM images identify the samples) (d). Normalized height distribution for the Ti6Al4V surfaces obtained with the different HF:EtOH solutions (the colours of the lines identify the corresponding AFM images) (e).

Figure 7.e shows the distribution of nanotopographic features and illustrates again that the sample etched in softer conditions (see green curve) exhibits a clearly different distribution, presenting a monodispersed profile with maximum value at 40 nm. At stronger etching conditions, the distribution presents also a maximum close to this value, but additional peaks with higher topography illustrate the increasing dispersion of the topographic distribution. These results are relevant to show that the sample obtained at lower HF concentrations presents a differentiating nanotopography with a smaller and more uniform distribution.

3.3 Response of OECs.

OECs were cultured on the surfaces of Ti6Al4V micropatterns obtained after irradiation with 10^{15} cm^{-2} and subsequent etching with different HF:EtOH solutions. The response was analysed by observation of the cells using fluorescence microscopy after GFP and nuclear staining. The results show that OECs adhere to all the substrates with no apparent differences in their capacity to extend filopodia (see figure 8a-c). In order to confirm the role of the actin cytoskeleton in the adhesion of the cells, an additional experiment was performed on Ti6Al4V micropatterns obtained with 1:4 HF:EtOh. The images obtained after staining with phalloidin-Alexa 647 confirmed that the expression of the actin cytoskeleton is rather peripheral and in coincidence with the edges and

terminations of the cell filopodia (See red staining in Figure 8.d), which suggests their indirect role in cell adhesion mechanisms.

A morphometric study was performed to elucidate differences between the interaction of OECs with the supports. We first observed a higher proportion of nuclei positioned over irradiated areas for the samples etched in the most concentrated HF (Figure 8.d). With Ti6Al4V surfaces prepared at the lowest HF concentration, we observed a remarkable increase in the proportion of nuclei positioned on the edges/interfaces between the masked/irradiated regions, suggesting that OECs are sensitive to the increasing lateral step quantified by AFM. The nucleus (denser part of the cell) tends to appear on masked/shaded areas at a step below the irradiated areas, especially for samples prepared at the stronger etching conditions. On the other hand, on Ti6Al4V surfaces with no evident topographic step between the shaded/irradiated areas (those obtained at the lowest HF concentration) nuclei appear most often at the interface/edge between the two contrasting areas.

We further performed a vectorial analysis of cell adhesion with respect to the orientation of the underlying micropattern to determine the influence of the substrate on OEC polarization (Figure 8.e). Paradoxically, the substrates showing less sensitivity to nuclear localization (i.e. those prepared with the lowest HF concentration) exhibited the highest induction of cell polarization in the direction of the underlying micropattern. Relevantly, this observation is accompanied by a tendency of the cells to adhere through divergent terminations on irradiated areas (brighter green background). According to the topographic study, these irradiated areas exhibit a flatter structure when confronted with the pitting surface of the masked areas. As further support of this, note the white arrows indicating areas of irradiated Ti6Al4V. These areas concentrate high densities of ramified adhesive terminations of OECs and long cytoskeletal extensions.

Relevantly, the inhibiting role of nanotopographic structures on the formation of focal adhesions has already been described for titania surfaces, which become antifouling [7]. The current results obtained on Ti6Al4V micropatterns indicate that nanotopographic features have an analogous inhibitory effect on the ability of OECs to adhere to these substrates. The inhibitory role of the nanotopography on the adhesion and its constriction to microscale areas induce a polarization of the cells.

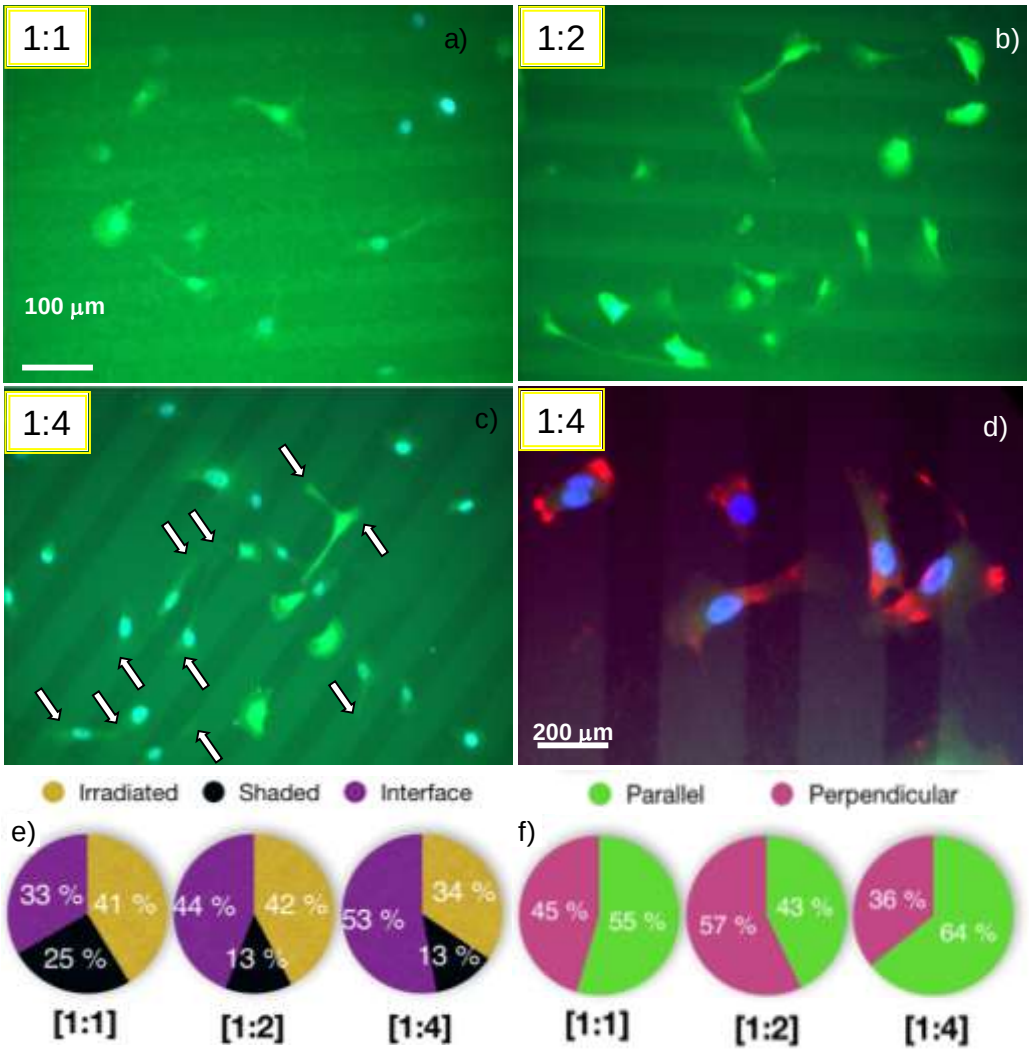

Fig 8: Adhesion of OECs on Ti6Al4V micropatterns obtained after irradiation with 10^{15} cm^{-2} and etching with HF:EtOH solutions of 1:1 (a), 1:2 (b) and 1:4 (c) (Green: GFP expression, Blue: DAPI). d) Actin cytoskeleton and nuclear staining of cells on Ti6Al4V

micropatterns etched in 1:4 HF:EtOH. e) Chart depicting statistics of location of OEC nuclei. f) Chart depicting statistics of OEC polarization.

4 Conclusions

The present work highlights the potential of the combination of sequential processes of selective ion beam irradiation and wet-etching for the engineering of micro-patterned Ti6Al4V surfaces of biomedical interest. We have shown that the irradiation induced damage and subsequent atmospheric exposure induces an oxidation of the surface, which is at the origin of a change in the surface wettability of Ti6Al4V. This change leads to a differential pitting on selectively irradiated Ti6Al4V after HF etching. Both pristine and irradiated Ti6Al4V surfaces are prone to pitting, but the etching evolves faster on pristine areas. Furtheremore, the wet-etching of irradiated Ti6Al4V leads to a surface enrichment in oxidized Al species. By increasing the surface tension of HF (i.e. higher EtOH concentration) and shortening the etching time, the nanotopographic contrasts can be maximized. The contrasts consist of a lateral step at the edge of the original irradiation mask (smaller for EtOH diluted HF) and to a nanoscale pitting (smaller and tending to monodisperse for EtOH diluted HF). In overall, the ion irradiation step desensitizes Ti6Al4V to etching in HF and the control of the HF concentration and immersion time allow optimizing the nanotopographic contrasts.

The bio-functionality of resulting micropatterns has been studied by culturing OECs. The localization of OEC nuclei and the overall orientation of the cells with respect to the 1D micropatterns suggest that the most effective structures to influence cell behaviour are those exhibiting smaller and more pronounced monodisperse nanotopography on the non-irradiated Ti6Al4V. These results open the opportunity to create biomedical supports with hierarchical micro-nanostructures by combining ion

beam irradiation and chemical etching processes. These may be valuable tools as passive stimulators, not only for OECs, but also for a wide range of differentiated and un-differentiated cells.

Acknowledgements

Authors thank the CMAM technical staff for operating the tandem accelerator and Luis García Pelayo for his technical assistance during materials processing and characterization. The current research was funded by grant NanoNeuroDev (2017/EEUU/11) from Santander-Universidad and grant Bio2Dsense (CTQ2017-84309-C2-2-R) from the Government of Spain.

Data Availability

The raw/processed data required to reproduce these findings cannot be shared at this time due to technical or time limitations. Please contact the corresponding author who will make the data available upon request.

References

[1] A.R. McAndrew, P.A. Colegrove, C. Buhr, B.C.D. Flipo, A. Vairis, A literature review of Ti-6Al-4V linear friction welding, Progress in Materials Science, 92 (2018) 225-257.

[2] D.M. Brunette , P. Tengvall , M. Textor , P. Thomsen Titanium in Medicine, Springer Verlag, Berlin Heidelberg, 2001.

[3] M.B. Sanchez-Ilarduya, E. Trouche, R. Tejero, G. Orive, I. Reviakine, E. Anitua, Time-dependent release of growth factors from implant surfaces treated with plasma rich in growth factors, Journal of Biomedical Materials Research Part A, 101 (2013) 1478-1488.

[4] M. Wieland, M. Textor, N.D. Spencer, D.M. Brunette, Wavelength-dependent roughness: A quantitative approach to characterizing the topography of rough titanium surfaces, International Journal of Oral & Maxillofacial Implants, 16 (2001) 163-181.

[5] T. Pratap, K. Patra, Mechanical micro-texturing of Ti-6Al-4V surfaces for improved wettability and bio-tribological performances, Surface & Coatings Technology, 349 (2018) 71-81.

[6] K. Anselme, M. Bigerelle, B. Noel, A. Iost, P. Hardouin, Effect of grooved titanium substratum on human osteoblastic cell growth, Journal of Biomedical Materials Research, 60 (2002) 529-540.

[7] D. Gallach Perez, E. Punzon Quijorna, R. Sanz, V. Torres-Costa, J.P. Garcia Ruiz, M. Manso Silvan, Nanotopography enhanced mobility determines mesenchymal stem cell distribution on micropatterned semiconductors bearing nanorough areas, Colloids and Surfaces B-Biointerfaces, 126 (2015) 146-153.

[8] E. Punzon-Quijorna, V. Sanchez Vaquero, S. Rodriguez-Lopez, V.M. de la Prida, A. Climent Font, J.P. Garcia Ruiz, M. Hernandez-Velez, M. Manso Silvan, Polymerized nanoporous titania surfaces: modification of cell adhesion by acrylic acid functionalization, Composite Interfaces, 19 (2012) 251-258.

[9] R.I.M. Asri, W.S.W. Harun, M. Samykano, N.A.C. Lah, S.A.C. Ghani, F. Tarlochan, M.R. Raza, Corrosion and surface modification on biocompatible metals: A review, Materials Science & Engineering C-Materials for Biological Applications, 77 (2017) 1261-1274.

[10] F.S. Utku, Electrochemically designed interfaces: Electrical properties and morphology of micro-nanostructured Titania implant surfaces, Surface & Coatings Technology, 324 (2017) 546-551.

[11] F.L.A. Vega, J.J. Olaya, J.B. Ruiz, Synthesis and corrosion resistance of SiO2-TiO2-ZrO2-Bi2O3 coatings spin-coated on Ti6Al4V alloy, Ceramics International, 44 (2018) 2123-2131.

[12] M. Manso, M. Langlet, M. Fernandez, L. Vazquez, J.M. Martinez-Duart, Surface and interface analysis of hydroxyapatite/TiO2 biocompatible structures, Materials Science & Engineering C-Biomimetic and Supramolecular Systems, 23 (2003) 451-454.

[13] R.A. Farghali, A.M. Fekry, R.A. Ahmed, H.K.A. Elhakim, Corrosion resistance of Ti modified by chitosan-gold nanoparticles for orthopedic implantation, International Journal of Biological Macromolecules, 79 (2015) 787-799.

[14] J.Q. Li, X. Lin, P.F. Guo, M.H. Song, W.D. Huang, Electrochemical behaviour of laser solid formed Ti-6Al-4V alloy in a highly concentrated NaCl solution, Corrosion Science, 142 (2018) 161-174.

[15] M. Kheradmandfard, S.F. Kashani-Bozorg, C.L. Kim, A.Z. Hanzaki, Y.S. Pyoun, J.H. Kim, A. Amanov, D.E. Kim, Nanostructured beta-type titanium alloy fabricated by ultrasonic nanocrystal surface modification, Ultrasonics Sonochemistry, 39 (2017) 698-706.

[16] L.C. Zhang, Y.J. Liu, S.J. Li, Y.L. Hao, Additive Manufacturing of Titanium Alloys by Electron Beam Melting: A Review, Advanced Engineering Materials, 20 (2018) 16.

[17] M. Manso-Silvan, J.M. Martinez-Duart, S. Ogueta, P. Garcia-Ruiz, J. Perez-Rigueiro, Development of human mesenchymal stem cells on DC sputtered titanium

nitride thin films, Journal of Materials Science-Materials in Medicine, 13 (2002) 289-293.

[18] M.S. Oskooie, M.S. Motlagh, H. Aghajani, Surface properties and mechanism of corrosion resistance enhancement in a high temperature nitrogen ion implanted medical grade Ti, Surface & Coatings Technology, 291 (2016) 356-364.

[19] M.P. Carroll, K. Stephenson, K.O. Findley, Characterization of high energy ion implantation into Ti-6Al-4V, Journal of Nuclear Materials, 389 (2009) 248-253.

[20] L.R. de la Vega, R. Trejo-Luna, J. Rickards, L. Banos, C. Falcony, The effects of implanting various high energy ions into Ti and Ti-6Al-4V, Surface & Coatings Technology, 196 (2005) 257-261.

[21] L. Csaderova, E. Martines, K. Seunarine, N. Gadegaard, C.D.W. Wilkinson, M.O. Riehle, A Biodegradable and Biocompatible Regular Nanopattern for Large-Scale Selective Cell Growth, Small, 6 (2010) 2755-2761.

[22] A. Curtis, C. Wilkinson, Topographical control of cells, Biomaterials, 18 (1997) 1573-1583.

[23] J.J. Wu, J.A. Li, F. Wu, Z.K. He, P. Yang, N. Huang, Effect of micropatterned TiO2 nanotubes thin film on the deposition of endothelial extracellular matrix: For the purpose of enhancing surface biocompatibility, Biointerphases, 10 (2015) 04A302.

[24] C. Liu, Y. Zhou, M. Sun, Q. Li, L.Q. Dong, L. Ma, K. Cheng, W.J. Weng, M.F. Yu, H.M. Wang, Light-Induced Cell Alignment and Harvest for Anisotropic Cell Sheet Technology, Acs Applied Materials & Interfaces, 9 (2017) 36513-36524.

[25] K.H. Cheon, C. Gao, M.H. Kang, H.D. Jung, T.S. Jang, H.E. Kim, Y.N. Li, J.H. Song, A crack-free anti-corrosive coating strategy for magnesium implants under deformation, Corrosion Science, 132 (2018) 116-124.

[26] V. Dumas, A. Guignandon, L. Vico, C. Mauclair, X. Zapata, M.T. Linossier, W. Bouleftour, J. Granier, S. Peyroche, J.-C. Dumas, H. Zahouani, A. Rattner, Femtosecond laser nano/micro patterning of titanium influences mesenchymal stem cell adhesion and commitment, Biomedical Materials, 10 (2015) 055002.

[27] T.N. Lerner, L. Ye, K. Deisseroth, Communication in Neural Circuits: Tools, Opportunities, and Challenges, Cell, 164 (2016) 1136-1150.

[28] V. Garcia-Escudero, R. Gargini, M.T. Gallego-Hernandez, A. Garcia-Gomez, M.J. Martin-Bermejo, D. Simon, A. Delicado, M.T. Moreno-Flores, J. Avila, F. Lim, A Neuroregenerative Human Ensheathing Glia Cell Line With Conditional Rapid Growth, Cell Transplantation, 20 (2011) 153-166.

[29] R.M. Gomez, M.Y. Sanchez, M. Portela-Lomba, K. Ghotme, G.E. Barreto, J. Sierra, M.T. Moreno-Flores, Cell therapy for spinal cord injury with olfactory ensheathing glia cells (OECs), Glia, 66 (2018) 1267-1301.

[30] R. Yao, M. Murtaza, J.T. Velasquez, M. Todorovic, A. Rayfield, J. Ekberg, M. Barton, J. St John, Olfactory Ensheathing Cells for Spinal Cord Injury: Sniffing Out the Issues, Cell Transplantation, 27 (2018) 879-889.

[31] J.F. Ziegler, M.D. Ziegler, J.P. Biersack, SRIM - The stopping and range of ions in matter (2010), Nuclear Instruments & Methods in Physics Research Section B-Beam Interactions with Materials and Atoms, 268 (2010) 1818-1823.

[32] I. Horcas, R. Fernandez, J.M. Gomez-Rodriguez, J. Colchero, J. Gomez-Herrero, A.M. Baro, WSXM: A software for scanning probe microscopy and a tool for nanotechnology, Review of Scientific Instruments, 78 (2007) 013705.

[33] M. Arroyo-Hernandez, J. Perez-Rigueiro, M. Manso-Silvan, J.M.M. Duart, Bioactivity test for amine-based functionalized meso- and macro-porous silicon

substrates, Materials Science & Engineering C-Biomimetic and Supramolecular Systems, 27 (2007) 1211-1214.

[34] M.F. Lopez, A. Gutierrez, J.A. Jimenez, Surface characterization of new non-toxic titanium alloys for use as biomaterials, Surface Science, 482 (2001) 300-305.

[35] Y.Z. Liu, X.T. Zu, C. Li, S.Y. Qiu, X.Q. Huang, L.M. Wang, Surface characteristics and corrosion behavior of Ti-Al-Zr alloy implanted with Al and Nb, Corrosion Science, 49 (2007) 1069-1080.

[36] M.F. Lopez, L. Soriano, F.J. Palomares, M. Sanchez-Agudo, G.G. Fuentes, A. Gutierrez, J.A. Jimenez, Soft x-ray absorption spectroscopy study of oxide layers on titanium alloys, Surface and Interface Analysis, 33 (2002) 570-576.

[37] B. Subramanian, R. Ananthakumar, M. Jayachandran, Microstructural, mechanical and electrochemical corrosion properties of sputtered titanium-aluminum-nitride films for bio-implants, Vacuum, 85 (2010) 601-609.